Intermetallics 59 (2015) 1–7

Contents lists available at ScienceDirect

Intermetallics

journal homepage: www.elsevier.com/locate/intermet

Thermal conductivity of Ni_3V–Ni_3Al pseudo-binary alloys

Satoshi Semboshi [a, b, *], Hiroyuki Tsuda [b], Yasuyuki Kaneno [b], Akihiro Iwase [b], Takayuki Takasugi [b]

[a] Kansai Center, Institute for Materials Research, Tohoku University, Gakuen-cho 1-1, Naka-ku, Sakai, Osaka 599-8531, Japan
[b] Department of Materials Science, Osaka Prefecture University, Gakuen-cho 1-1, Naka-ku, Sakai, Osaka 599-8531, Japan

ARTICLE INFO

Article history:
Received 27 August 2014
Received in revised form
7 December 2014
Accepted 10 December 2014
Available online

Keywords:
A. Intermetallics
B. Thermal properties
D. Microstructure
E. Physical properties

ABSTRACT

The effect of changes in the composition and microstructure of the Ni_3V–Ni_3Al pseudo-binary alloys on their thermal conductivity has been investigated. For Ni_3V and Ni_3Al-based single-phase alloys, the thermal conductivity shows a maximum value at the stoichiometric compositions, and it decreases as the V (or Al) content of the Ni_3Al (or Ni_3V) alloy increases, following the Nordheim rule. For Ni_3V–Ni_3Al two-phase alloys, the thermal conductivity of the constituent Ni_3Al phase exhibits a smaller value than that of the Ni_3V phase. Eventually, the thermal conductivity of the two-phase alloys decreases as the Al content increases because of the increase in the volume fraction of the Ni_3Al phase with low conductivity. As the temperature increases from 293 K to 1073 K, the conductivity increases for all of the alloys but not for stoichiometric Ni_3V. However, the dependence of the thermal conductivity on the alloy composition between 293 K and 1073 K is similar. Hence, it is confirmed that the thermal conductivity of the Ni_3V–Ni_3Al pseudo-binary alloys is controlled by the composition and volume fraction of the constituent phase.

1. Introduction

Intermetallic Ni_3X (X = Al, Si, Ti, V, and Nb) based alloys comprise geometrically closed-packed face-centered cubic (fcc) $L1_2$, hexagonal $D0_{19}$, tetragonal $D0_{22}$, and hexagonal D0a structures. They have been attracting attention for use in parts of aero-engines or industrial gas turbines that are subjected to high temperatures and an oxidizing atmosphere [1–4]. In particular, Ni_3Al-based alloys are advantageous for high-temperature applications owing to the enhanced mechanical properties with increasing temperature (referred to as the anomalous temperature dependency of yielding [5,6]). Recently, so-called dual two-phase intermetallic alloys, based on the Ni_3V–Ni_3Al pseudo-binary system, have been shown to exhibit very attractive properties, suitable as high-temperature structural materials [7–9]. Fig. 1 shows the phase diagram of the Ni_3V–Ni_3Al pseudo-binary system, in which a eutectoid reaction is shown to occur at 1281 K [10,11]. As the temperature decreases in the hyper-eutectoid compositional range, the constituent phases of the alloys changes from the fcc solid solution (A1) phase at high temperatures below the melting point, through the two-phase field of fcc (Al) and Ni_3Al ($L1_2$) at intermediate temperatures, and finally to the two-phase field of Ni_3V ($D0_{22}$) and Ni_3Al ($L1_2$) at temperatures below the eutectoid temperature. The resulting microstructure of the alloys is composed of primary cuboidal Ni_3Al precipitates surrounded by channel regions with fine lamellar microstructure, where the previous A1 phase decomposes into Ni_3V ($D0_{22}$) and Ni_3Al phases, as illustrated in Fig. 2. The alloys have high phase stability and show coherent microstructures that coexist between individual constituent phases. Accordingly, these alloys have excellent mechanical strengths at high temperatures; e.g., they exhibit more than 1000 MPa in tensile strength at 1073 K, which is competitive to that of conventional super alloys [8].

There has been much effort to further enhance the mechanical properties of Ni_3V–Ni_3Al two-phase alloys and to understand their microstructural and compositional features [7,8,12,13]. On the other hand, to obtain the reliability required for high-temperature structural products, the thermal conductivity is also an important criterion when selecting an appropriate material. Materials engineered for turbine blades are expected to exhibit high thermal conductivity that guarantees low thermal gradients of the components, which results in lower thermal stresses and in a longer life-time and superior resistance against thermal fatigue. However, measurements of the thermal conductivity of Ni_3V–Ni_3Al two-

* Corresponding author. Kansai Center, Institute for Materials Research, Tohoku University, Gakuen-cho 1-1, Naka-ku, Sakai, Osaka 599-8531, Japan. Tel.: +81 72 252 1161x5700; fax: +81 72 254 9912.
E-mail address: semboshi@imr.tohoku.ac.jp (S. Semboshi).

http://dx.doi.org/10.1016/j.intermet.2014.12.006
0966-9795/

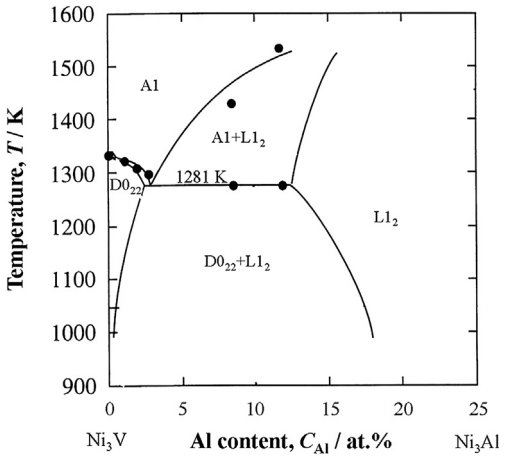

Fig. 1. Ni_3V–Ni_3Al pseudo-binary phase diagram [11].

phase alloys have been confirmed so far only for selected microstructure, composition, and temperature [14]. In this study, we comprehensively surveyed the thermal conductivity of Ni_3V–Ni_3Al pseudo-binary alloys, including not only two-phase alloys but also single-phase Ni_3Al and Ni_3V. The effects of the composition and microstructure in the constituent phases on the thermal conductivity were investigated. The temperature dependence of the thermal conductivity, which is important for applications at elevated temperatures, was also examined between 293 K (i.e., room temperature) and 1073 K.

2. Experimental

Button ingots of Ni_3V–Ni_3Al pseudo-binary alloys were fabricated by arc-melting in argon atmosphere using 99.99 wt.% nickel, 99.99 wt.% aluminum, and 99.9 wt.% vanadium tips as raw materials; melting was performed out four times to attain compositional homogeneity. We prepared thirteen Ni–$(25 - x)$ at.% V – x at.% Al alloys with nominal compositions of $x = 0$, 2.5, 5, 7, 8, 9, 10, 11, 12.5, 15, 17.5, 20, and 25. These alloys are hereby designated by the Al content x; for example, the Ni–22.5 at.% V–2.5 at.% Al alloy is referred to as the "2.5 Al alloy". The alloys were homogenized at 1553 K for 3 h in vacuum and then cooled in the furnace. Thereafter, the alloys were cut into plate-shaped specimens (measuring 20 mm in length, 2 mm in width, and 1 mm in thickness) and disk-shaped specimens (measuring 10 mm in diameter and 1.5 mm in thickness) employing electrical-discharge machining. The plate-shaped specimens were used for electron-microscopy observations, and the disk-shaped specimens were used for thermal-conductivity measurements.

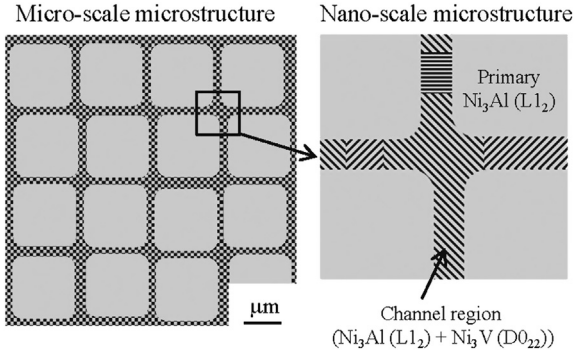

Fig. 2. Illustration of the microstructure of the Ni_3Al–Ni_3V dual two-phase alloys.

The microstructures of the specimens were observed with a field-emission scanning electron microscope (FE-SEM; SU8000, Hitachi) operating at 15 kV, and a transmission electron microscope equipped with an energy-dispersive X-ray spectrometer (TEM-EDX; Titan, FEI) operating at 300 kV. For the FE-SEM-based microstructural observations, the specimens were mechanically polished using 2000-grade emery paper and then electrochemically polished with a solution of 15 vol.% sulfuric acid and 85 vol.% methanol at 258 K, at an applied DC voltage of 15 V for 20 s. For the TEM-based microstructural observations, the disk-shaped specimens were ground to thin, foil-like samples with a thickness of less than 50 μm. They were then subjected to low-angle ion milling using an argon ion beam accelerated at voltages below 3 kV. High-purity (6N) argon gas was used as argon ion-beam source.

The thermal diffusivity, α, and heat capacity, C_p, were measured by the laser-flash method at temperatures between 293 K and 1073 K using a thermal constant analyzer (TC-8000, ULVAC-RIKO). The specimen surface was covered with graphite powder to ensure sensitive response to the thermal flow detected by an infrared sensor. A short-duration laser pulse, whose wavelength was approximately 700 nm, was emitted from a sapphire rod onto the surface of the specimen. The values of α and C_p were analyzed from the time dependent thermal profile of the surface opposite to the irradiated side of the specimen. The thermal conductivity λ was calculated from α, C_p, and the density ρ, using the following equation:

$$\lambda = \alpha \times Cp \times \rho_0 \quad (1)$$

The density ρ_0 of each alloy was obtained from the size and weight of the disc-shaped specimens. Details of the laser-flash apparatus and measuring principle of the thermal conductivity have been reported in Refs. [15–17].

3. Results

3.1. Microstructure

Fig. 3 shows FE-SEM images of the microstructures of the 2.5, 5, 7, 10, 12.5, and 15 Al alloys. The 0 and 2.5 Al alloys exhibited a single Ni_3V phase with a typical lamellar structure, as shown in Fig. 3(a), which was also observed in previous studies [18]. The microstructure of the 5 Al alloy could not be resolved from the FE-SEM image, as evident from Fig. 3(b). Fig. 4 shows a bright-field (BF) TEM image and selected area electron diffraction (SAED) patterns of the 5 Al alloy. A small amount of a cuboidal phase, marked by a solid circle in Fig. 4(a), is visible within the lamellar structures indicated by a dotted circle. The SAED pattern corresponding to the cuboidal phase (Fig. 4(b)) was identified to be the Ll_2 structure of Ni_3Al, and that corresponding to the lamellar structure (Fig. 4(c)) was identified as the $D0_{22}$ structure of Ni_3V, superimposed on the former structure. Thus, the microstructure observed in the 5 Al alloy corresponds to a hyper-composition slightly higher than the eutectoid composition, which is consistent with the phase diagram shown in Fig. 1. In the 7–12.5 Al alloys, two-phase microstructures consisting of the primary Ni_3Al phase and channel regions were clearly observed, as shown in Fig. 3(c–e). In the alloys whose Al content was above 15 at.%, the microstructure was dominated by a single-phase of Ni_3Al, as shown in Fig. 3(f).

Fig. 5 shows the volume fractions of the Ni_3Al and Ni_3V phases for alloys with different Al content. To obtain the volume fractions, we first measured the volume fractions of the primary Ni_3Al precipitates and the channel regions containing both Ni_3Al and Ni_3V phases by the point-count method using the FE-SEM images, as shown in Fig. 3. Next, the volume fraction of the two phases in the

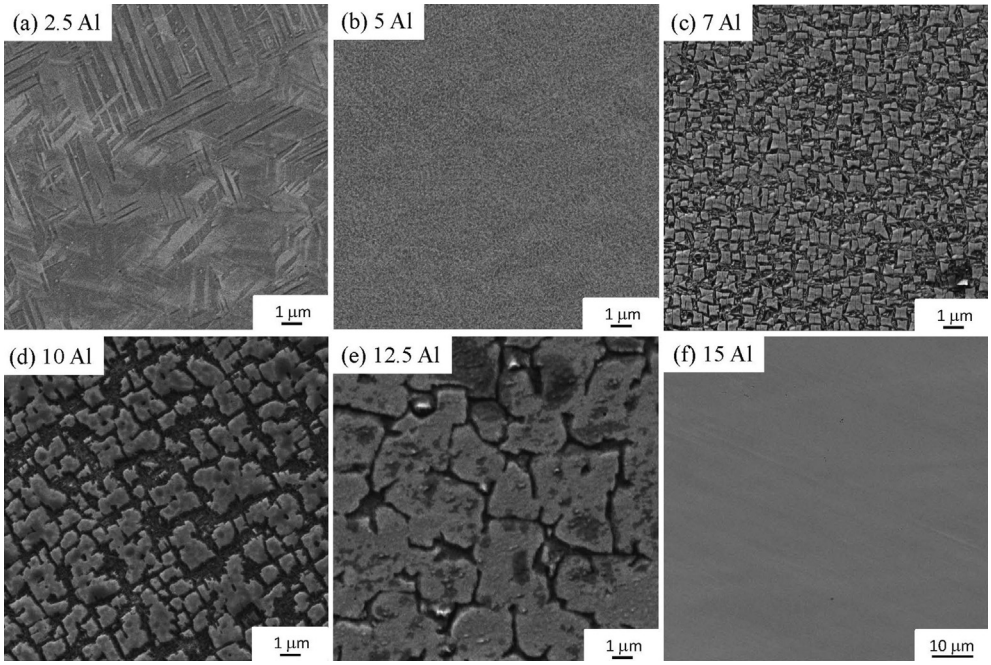

Fig. 3. FE-SEM micrographs of the (a) 2.5, (b) 5, (c) 7, (d) 10, (e) 12.5, and (f) 15 Al alloy.

channel regions was calculated from the tie line at the eutectoid temperature in the phase diagram shown in Fig. 1, according to the lever rule at equilibrium. For the Ni_3V–Ni_3Al two-phase alloys, i.e., alloys with Al content ranging between 7 and 12.5 at.%, the volume fraction of the Ni_3Al phase increased linearly with increasing Al content. Note that we excluded the data of the volume fraction for the 5 Al alloy because the corresponding FE-SEM image was blurred. Fig. 5 suggests that the solubility limit of Al in the Ni_3V phase was approximately 3 at.%, and that of V in the Ni_3Al phase was 10 at.%, which does not appears to be very far from the values shown in Fig. 1.

Table 1 lists the contents of the elements Ni, Al, and V in the Ni_3V and Ni_3Al phases of the 7, 9, and 11 Al alloys (i.e., two-phase alloys), which were analyzed by TEM-EDS measurements. It is noted that the compositions of the Ni_3V and Ni_3Al phases are almost identical in the three alloys. The compositions of the Ni_3V and Ni_3Al phases in these two-phase alloys were approximately Ni–3 at.% Al–22 at.% V and Ni–12 at.% Al–12 at.% V, respectively, although the precision of the contents on the basis of TEM-EDX remains controversial. These compositions are not significantly different from the result determined from the volume fractions shown in Fig. 5.

3.2. Thermal conductivity

Fig. 6(a) and (b) shows the thermal diffusivity α and heat capacity C_p of the pseudo-binary alloys, measured by the laser-flash

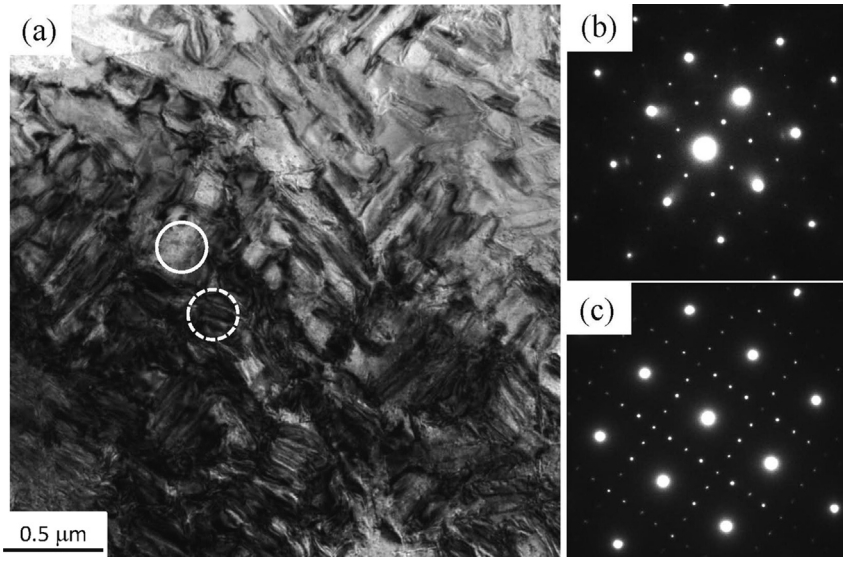

Fig. 4. (a) BF TEM image and (b, c) SAED patterns of the 5 Al alloy. The pattern in (b) was obtained from a cuboidal particle marked by the solid circle in (a), which was identified as the $L1_2$ structure of Ni_3Al. The pattern in (c) was obtained from the channel region marked by the dotted circle in (a), which was identified as superposition of the $D0_{22}$ structure of Ni_3V and the $L1_2$ structure of Ni_3Al. Note that the incident electron-beam directions in the SAED patterns were $[001]_{L12}$ and $[001]_{D022}$.

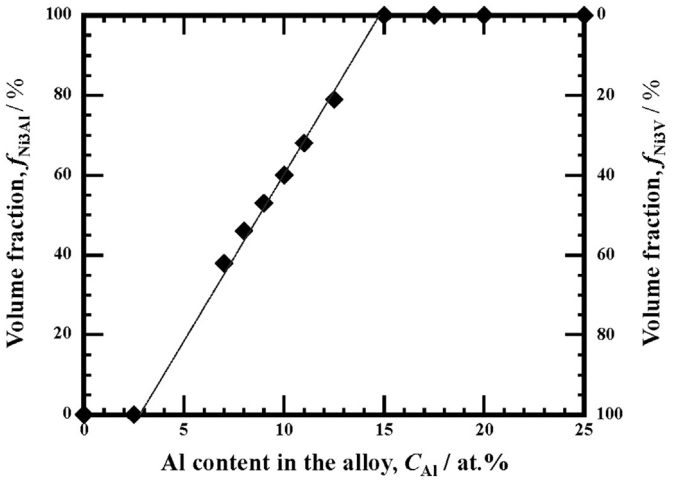

Fig. 5. Volume fractions of the constituent phases of the Ni_3V–Ni_3Al pseudo-binary alloys. The values were obtained from the total of the cuboidal precipitates, measured by the point-counting method from the FE-SEM micrographs as shown in Fig. 3, and the total of the channel regions calculated from the pseudo-binary phase diagram shown in Fig. 1.

method at 293 K. The value of α of the 0 Al alloy was 8.2×10^{-6} m^2/s. The value of α decreased to 4.1×10^{-6} m^2/s as the Al content rose to 12.5 at.%, above which it increased to 8.5×10^{-6} m^2/s. The heat capacity C_p appeared to either remain constant within the experimental accuracy or to increase slightly as the Al content increased. Fig. 6(c) shows the measured density ρ_0 of the pseudo-binary alloys together with values calculated from the lattice parameter and weight of the unit cell of the constituent phases. In the case of two-phase alloys, the alloy density was determined by combining the density of the constituent phases and their corresponding volume fraction (see Fig. 5). The measured ρ_0 decreases as the Al content increases, which is in good agreement with the calculated values.

Fig. 6(d) shows the thermal conductivity at 293 K, λ_{293}, calculated from Eq. (1), together with the data previously reported by Terada et al. [19,20]. The λ_{293} values for the stoichiometric Ni_3V and Ni_3Al intermetallic compound were measured to be 31 and 29 W/mK, respectively, which are close to previously reported data (marked by open circles in Fig. 6(d)). In the single-phase regions of Ni_3V (and Ni_3Al), λ_{293} decreased with increasing Al (and V) content. In the Ni_3V and Ni_3Al two-phase region, λ_{293} steadily decreased with increasing Al content and appeared to coincide with the values at the solubility limits of the Ni_3V and Ni_3Al phases.

Fig. 7 shows the temperature dependence of the thermal conductivity of the 0, 7, 11, 15, and 25 Al alloys. The thermal conductivity of the 0 Al alloy decreased gradually with increasing temperature, whereas those of the other alloys showed a monotonic increase with temperature. We can roughly conclude from Fig. 7 that the thermal conductivity increased monotonically with temperature. These plots demonstrate that the thermal conductivities of the stoichiometric compounds Ni_3V and Ni_3Al (i.e., the 0 and 25 Al alloys, respectively) were relatively insensitive against temperature compared to other alloys, whose behavior has been explained in previous reports [19,21], corresponding to Mooiji's rule in case of the electrical resistivity [22]. As shown in the Appendix, the thermal conductivity and resistivity of the Ni_3V–Ni_3Al pseudo-binary alloys were gauged with the electrical conductivity and resistivity, and their correspondence could be explained by free-electron theory. The thermal conductivity at 1073 K, λ_{1073}, of all investigated the alloys is also plotted in Fig. 6(d) and reveals that the value of λ_{1073} varied with the Al content in a manner similar to that of λ_{293}.

Fig. 8 shows the temperature coefficient of the thermal conductivity β as a function of the Al content of the Ni_3V–Ni_3Al pseudo-binary alloys, calculated by the least-squares method for the conductivity–temperature relationship shown in Fig. 7. In the single-phase region of Ni_3V (or Ni_3Al), β steeply increased with increasing Al (or V) content. In the Ni_3V and Ni_3Al two-phase region, β slowly increased with increasing Al content and almost coincided with the values at the solubility limits of the Ni_3V and Ni_3Al phases.

Table 1
Ni, Al, and V content in the Ni_3V and Ni_3Al phases of the 7, 9, and 11 Al alloys, determined by TEM-EDX measurements.

		Ni/at.%	Al/at.%	V/at.%
7 Al alloy	Ni_3V	75.3 ± 1.0	2.8 ± 0.4	21.9 ± 0.9
	Ni_3Al	76.3 ± 1.0	12.0 ± 0.8	11.7 ± 0.4
9 Al alloy	Ni_3V	75.5 ± 1.4	2.9 ± 0.9	21.6 ± 2.1
	Ni_3Al	76.7 ± 0.6	11.6 ± 0.5	11.7 ± 0.3
11 Al alloy	Ni_3V	75.4 ± 0.6	2.7±1.1	21.9 ± 1.5
	Ni_3Al	76.3 ± 0.7	11.5 ± 0.6	12.2 ± 0.3

4. Discussion

In this section, the relationship between the microstructure and thermal conductivity of the Ni_3V–Ni_3Al pseudo-binary alloys is discussed in detail. As confirmed by Figs. 3 and 5, the alloys can be divided into three microstructural groups: (i) the 0 to 2.5 Al alloys comprising the Ni_3V single-phase microstructure, (ii) the 5 to 12.5 Al alloys comprising the Ni_3V–Ni_3Al two-phase microstructure, and (iii) the 15–25 Al alloys comprising the Ni_3Al single-phase microstructure. It can be considered that the distribution of the elements in the constituent phases principally followed Gibbs phase rule of the Ni_3V–Ni_3Al pseudo-binary system, although the present alloys actually presented the ternary Ni, V, and Al system. This approach was justified by the fact that the compositions of the constituent phases Ni_3Al and Ni_3V were almost identical in all investigated two-phase alloys (see Table 1), as well as the increase in volume fraction of the Ni_3Al phase with increasing Al content.

As described earlier, within the single-phase region of Ni_3V (or Ni_3Al), the thermal conductivity of the alloys decreased with increasing Al (or V) content at temperatures from 293 to 1073 K (see Fig. 6(d)). Fig. 9 shows the thermal resistivity ρ at 293 K and 1073 K for the Ni_3V and Ni_3Al single-phase alloys as a function of the Al content. Here, ρ was calculated as the inverse of the thermal conductivity shown in Fig. 6(d). We can see in Fig. 9(b) that there is a linear relationship between ρ and the amount of V (C_V [at.%]) in the Ni_3Al single-phase alloys, following Nordheim's rule with respect to the electrical resistivity [23,24]. Therefore, when the Al sites in the Ni_3Al single-phase alloys were replaced by V atoms, the thermal conductivity λ_{Ni_3Al} at 293 K and 1073 K can be approximately obtained from the experimental results using the following equation:

$$1/\lambda_{Ni_3Al/293K} = \rho_{Ni_3Al/293K} = 0.0035C_V + 0.0341 \ [mK/W]$$
$$1/\lambda_{Ni_3Al/1073K} = \rho_{Ni_3Al/1073K} = 0.0020C_V + 0.0309 \ [mK/W] \quad (2)$$

C_V is the concentration of V [at.%] in the Ni_3Al phase. The thermal conductivity of the Ni_3V single-phase alloys λ_{Ni_3V} is also given by the following equation using the data of Fig. 9(a), although the accuracy of their equation requires verification because it is based on only two experimental data points.

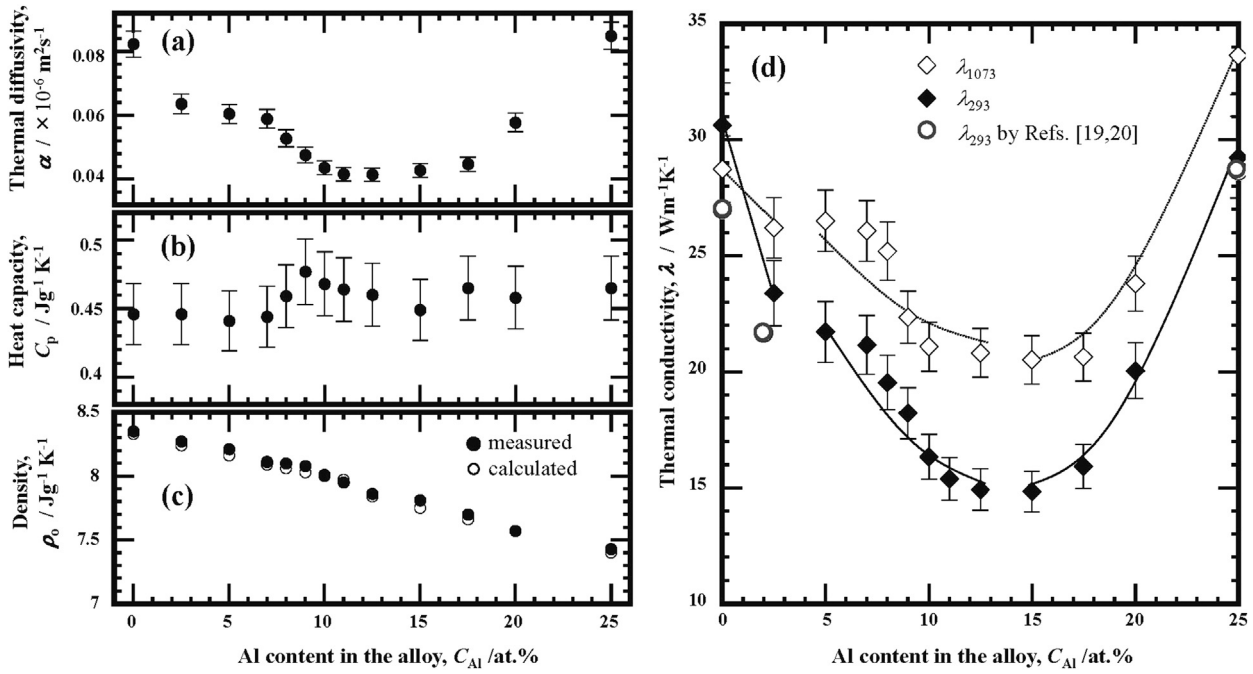

Fig. 6. Variations in the (a) thermal diffusivity, (b) heat capacity, (c) density, and (c) thermal conductivity at 293 K as a function of the Al content of the Ni_3V–Ni_3Al pseudo-binary alloys, together with previously reported data [19,20]. The conductivities measured at 1073 K are also plotted in (d) and are represented by open diamonds.

$$1/\lambda_{Ni_3V/293K} = \rho_{Ni_3V/293K} = 0.0040C_{Al} + 0.0326 \ \text{[mK/W]}$$
$$1/\lambda_{Ni_3V/1073K} = \rho_{Ni_3V/1073K} = 0.0006C_{Al} + 0.0328 \ \text{[mK/W]} \quad (3)$$

C_{Al} is the concentration of Al [at.%] in the Ni_3V phase. These results confirm that the thermal conductivity becomes less dependent on composition at higher temperatures for both Ni_3V and Ni_3Al single-phase alloys.

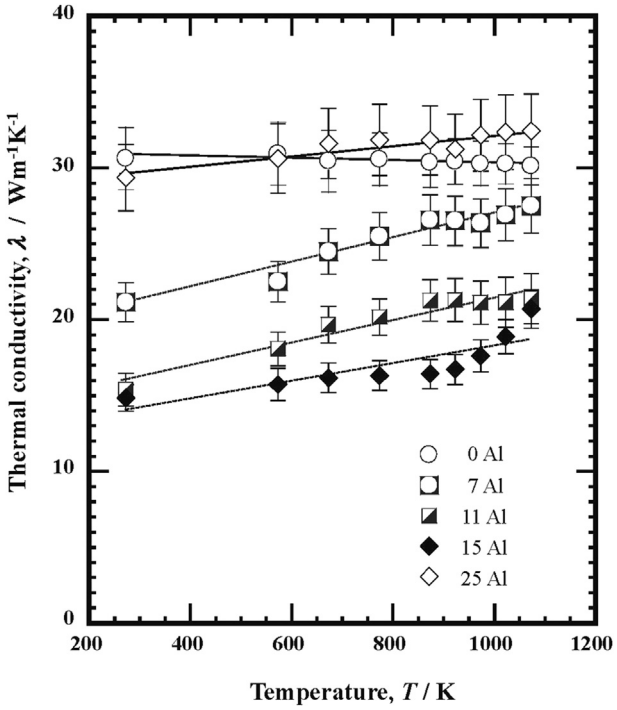

Fig. 7. Temperature dependence of the thermal conductivity of the 0 (i.e., stoichiometric Ni_3V), 7, 11, 15, and 25 Al (i.e., stoichiometric Ni_3Al) alloys.

In two-phase alloys of a binary system, the thermal conductivity is known to be determined by the microstructure, such as the volume fraction and distribution of the constituent phases, because the individual phase composition in the alloys is constant, according to Gibbs phase rule. Assuming that a simple spherical second phase is homogeneously distributed in the two-phase alloys, the thermal conductivity λ is given by the following equation [25]:

$$\lambda = \frac{3}{4}\left[\left(f_1 - \frac{1}{3}\right)\lambda_1 + \left(f_2 - \frac{1}{3}\right)\lambda_2 + \sqrt{\left\{\left(f_1 - \frac{1}{3}\right)\lambda_1 + \left(f_2 - \frac{1}{3}\right)\lambda_2\right\}^2 + \frac{8}{9}\lambda_1\lambda_2}\right] \quad (4)$$

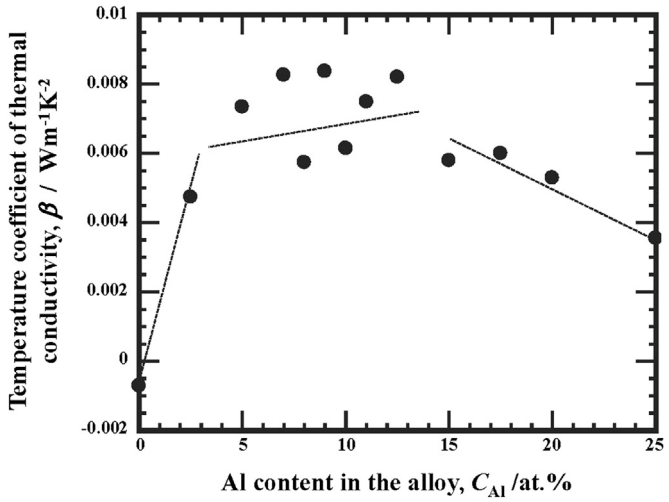

Fig. 8. Temperature coefficient of the thermal conductivity as a function of the Al content of the Ni_3V–Ni_3Al pseudo-binary alloys, obtained from the correlation between thermal conductivity and temperature shown in Fig. 7.

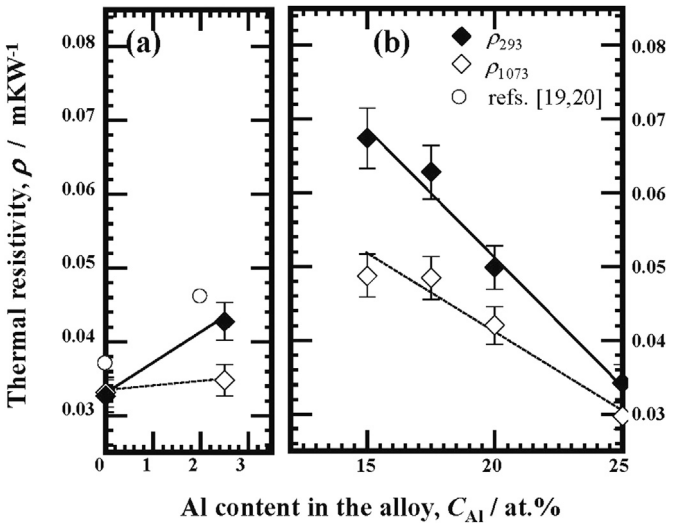

Fig. 9. Thermal resistivity at 293 and 1073 K as a function of the Al content of (a) Ni_3V and (b) Ni_3Al single-phase alloys, together with the values reported in previous studies [19,20]. The values were calculated using Eqs. (2) and (3).

f_1 and f_2 are the volume fractions, and λ_1 and λ_2 are the thermal conductivities of the matrix and second phase, respectively. In the case of the Ni_3V–Ni_3Al two-phase alloys, the λ_{Ni_3Al} and λ_{Ni_3V} can be approximately calculated to be 14 and 23 W/mK, respectively, from Eqs. (2) and (3) using the solubility limit of V in the Ni_3Al phase (10 at.%) and that of Al in the Ni_3V phase (3 at.%), as seen in Fig. 5. Fig. 10 shows the thermal conductivities at 293 K and 1073 K for the Ni_3V–Ni_3Al two-phase alloys as a function of the volume fraction of the Ni_3Al phase, together with the curves derived from Eq. (4) for λ_{293} and λ_{1073}. Fig. 10 reveals good agreement between measured and calculated thermal conductivity, even though the calculation was based on rough estimations.

Thus, the premise underlying Eq. (4) is not an odd explanation of the thermal conductivity in the region of the Ni_3V–Ni_3Al two-phase microstructure: the decrease in thermal conductivity with increasing Al content of the two-phase alloys can be explained by the increasing volume fraction of the constituent Ni_3Al phase, which had a smaller thermal conductivity than the Ni_3V phase. The

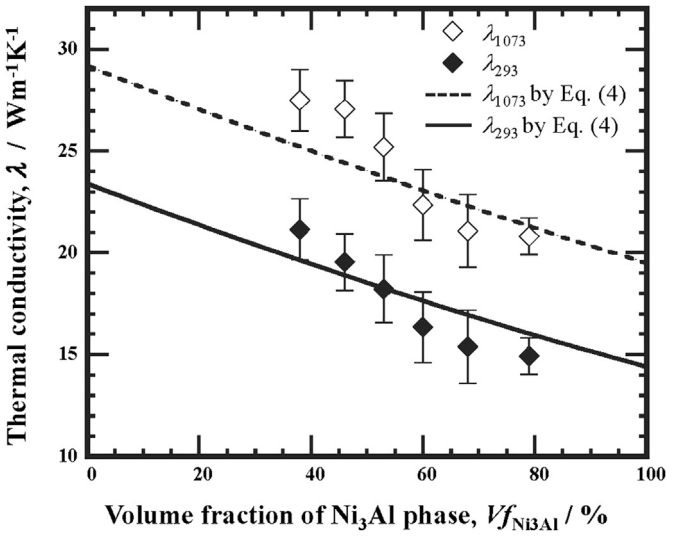

Fig. 10. Thermal conductivity at 293 K and 1073 K as a function of the Al content of the Ni_3V–Ni_3Al two-phase alloys.

smaller conductivity of the constituent Ni_3Al phase is attributed to a large amount of substituting V atoms at Al sites (approximately 10 at.%), which significantly decreased the thermal conductivity of stoichiometric Ni_3Al (29 W/m K). It should be noted that at the interface between the Ni_3V and Ni_3Al phase, especially in the channel regions, the thermal conductivity might be decreased. It is, however, speculated that the contribution of the interface to the thermal conductivity should be small (at least within the limit of the present experimental accuracy), because the thermal conductivity seems to vary continuously throughout the entire compositional range of the alloys.

According to the findings obtained in this study, in order to increase the thermal conductivity of the two-phase alloys, the volume fraction of the Ni_3Al phase or the substitutional content of V (or Al) in the Ni_3Al (or Ni_3V) phase, or both parameters must be decreased effectively. For example, heat-treatment at a temperature below the eutectoid temperature of 1281 K could be a promising route, and the results will be confirmed and reported in a future paper.

5. Summary

The effect of composition and microstructure on the thermal conductivity at temperatures from 293 to 1073 K were investigated for Ni_3V–Ni_3Al pseudo-binary alloys with various compositions of Ni–$(25-x)$ at.% V– x at.% Al ($0 < x < 25$). The alloys with 0–2.5 at.% Al and 15–25 at.% Al exhibited the Ni_3V and Ni_3Al single-phase microstructures, respectively. On the other hand, the alloys with 5–12.5 at.% Al consisted of primary cuboidal Ni_3Al precipitates and channeling regions containing fine Ni_3Al and Ni_3V phases. In the two-phase alloys, the volume fraction of the Ni_3Al phase increased linearly with increasing Al content.

In the two single-phase alloys, the thermal resistivity increased linearly with increasing deviation from stoichiometry, following the Nordheim rule, and the thermal conductivity decreased accordingly. In the Ni_3Al and Ni_3V two-phase alloys, the thermal conductivity of the alloys decreased with increasing Al content, which can be explained in terms of the conductivity and volume fraction of the constituent phases: an increase of the Al content in the alloys led to an increase in the volume fraction of the Ni_3Al phase, which had lower conductivity than the Ni_3V phase. It should be noted that the variation of the thermal conductivity as a function of the alloy composition is identical at the temperatures between 293 K and 1073 K, although the absolute value of the thermal conductivity increases as the temperature increases, with the exception of stoichiometric Ni_3V. Thus, it is concluded that the thermal conductivity of the Ni_3V–Ni_3Al pseudo-binary alloys is controlled by the composition and volume fraction of the constituent phase.

Acknowledgments

The authors are grateful to Prof. N. Masahashi of the Institute for Materials Research (IMR) at Tohoku University for useful discussions and comments. The authors also thank Mr. E. Aoyagi and Dr. T. Ashino of the IMR for their technical assistance. Financial support provided by the Japan Society for the Promotion of Science (JSPS) as a Grant-in-Aid for Scientific Research (C) (No. 26420663) is gratefully acknowledged.

Appendix. Relationship between thermal and electrical conductivities of Ni_3V–Ni_3Al pseudo-binary alloys

An empirical relationship between the thermal conductivity λ [W/mK] and electrical conductivity σ [m/Ω] has been adopted to

describe metallic alloys. With the exception of extremely low temperatures, the following equation based on the Wiedemann–Franz law can be used:

$$\lambda = AL_0T\sigma + B \quad \text{(A-1)}$$

L_0 is the Lorenz number ($L_0 = 2.45 \times 10^{-8}$ WΩ/K^2), T is the absolute temperature, and A and B are constants that are adjusted to fit the data. In the case of a Ni-based alloy, A and B have been reported to be 0.869 and 8.4 W/mK, respectively [26]. In the present study, the electrical conductivity of the Ni_3V–Ni_3Al pseudo-binary alloys was measured to confirm the relationship between their thermal and electrical conductivity. The values of the electrical conductivity of the alloys were obtained by measuring the electrical resistivity using the standard DC four-probe technique at room temperature. For these resistivity measurements, plate-shaped specimens with the dimension of 20 mm in length, 2 mm in width, and 1 mm in thickness were used.

Fig. A1 shows the experimental data of the Ni_3V–Ni_3Al pseudo-binary alloys investigated in this study, as well as the plots obtained from Eq. (A-l). As evident from Fig. A1, the experimental data reasonably coincided with the line derived from Eq. (A-l). This demonstrates that the thermal and electrical conductivities of the Ni_3V–Ni_3Al pseudo-binary alloys show conventional metallic behavior, according to the Wiedemann–Franz law.

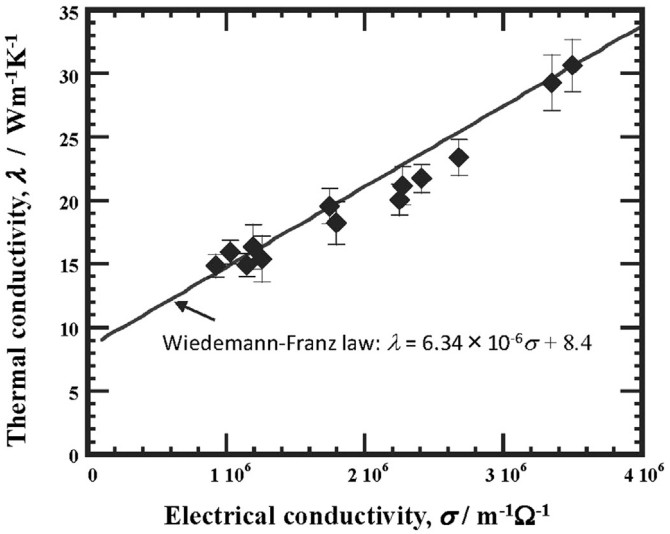

Fig. Al. Thermal and electrical conductivity of the Ni_3V–Ni_3Al pseudo-binary alloys at room temperature (293 K) fitted by the Wiedemann-Franz law (solid line) [26].

References

[1] Yamaguchi M, Inui H, Ito K. High-temperature structural intermetallics. Acta Mater 2000;48:307–22.

[2] Mazdiyasni S, Miracle DB, Dimiduk DM, Mendiratta MG, Subramanian PR. High temperature phase equilibria of the Ll_2 composition in the Al–Ti–Ni, Al–Ti–Fe, and Al–Ti–Cu systems. Scr Metall 1989;23:327–31.

[3] Yoo MH, Sass SL, Fu CL, Mills MJ, Dimiduk DM, George EP. Deformation and fracture of intermetallics. Acta Metall Mater 1993;41:987–1002.

[4] Liu CT, Stringer J, Mundy JN, Horton LL, Angelini P. Ordered intermetallics alloys: an assessment. Intermetallics 1997;5:579–96.

[5] Liu CT. Recent advances in ordered intermetallics. Mater Chem Phys 1995;42: 77–86.

[6] Caillard D. Yield-stress anomalies and high-temperature mechanical properties of intermetallics and disordered alloys. Mater Sci Eng A 2001;319–321: 74–83.

[7] Nunomura Y, Kaneno Y, Tsuda H, Takasugi T. Dual multi-phase intermetallic alloys composed of geometrically close-packed Ni_3X (X: Al, Ti and V) type structures – I. Microstructures and their stability. Acta Mater 2006;54: 851–60.

[8] Shibuya S, Kaneno Y, Yoshida M, Takasugi T. Dual multi-phase intermetallic alloys composed of geometrically close packed Ni_3X (X: Al, Ti and V) type structures – II. Mechanical properties. Acta Mater 2006;54:861–70.

[9] Mishima Y, Hong TM, Suzuki T. Determination of the γ solvus surface in Ni–Al–X ternary systems 1991;146:123–30.

[10] Hong TM, Mishima Y, Suzuki T. Accurate determination of γ′ solvus in Ni–Al–X ternary systems. In: Proc of Materials Research Society (MRS) symposium, 133. MRS; 1989. p. 429–33.

[11] Poduri R, Chen LQ. Computer simulation of atomic ordering and compositional clustering in the pseudobinary Ni_3Al–Ni_3V system. Acta Mater 1998;46:1719–29.

[12] Moronaga T, Ishii S, Kaneno Y, Tsuda H, Takasugi T. Aging effects on microstructure and hardness of two-phase Ni_3Al–Ni_3V intermetallic alloys containing Ta and Re. Mater Sci Eng A 2012;539:30–7.

[13] Kobayashi S, Sato K, Hayashi E, Osaka T, Konno TJ, Kaneno Y, et al. Alloying effects on the phase equilibria among Ni(A1), $Ni_3Al(L1_2)$ and $Ni_3V(D0_{22})$ phases. Intermetallics 2012;23:68–75.

[14] Takasugi T, Kaneno Y. Properties and application for two-phase intermetallics alloys composed of geometrically close packed Ni_3X (X: Al and V)) structure. MRS Symp Proc Publ 2009;1128:351–6.

[15] Terada Y, Ohkubo K, Nakagawa K, Mohri T, Suzuki T. Thermal conductivity of B2-type aluminides and titanides. Intermetallics 1995;3:347–55.

[16] Parker WJ, Jenkins RJ, Butler CP, Abbott GL. Flash method of determining thermal diffusivity, heat capacity and thermal conductivity. J Appl Phys 1961;32:1679–84.

[17] Min S, Blumm J, Lindemann A. A new laser flash system for measurement of the thermophysical properties. Thermochim Acta 2007;455:46–9.

[18] Suzuki A, Kojima H, Matsuo T, Takeyama M. Alloying effect on stability of multi-variant structure of Ni_3V at elevated temperatures. Intermetallics 2004;12:969–75.

[19] Terada Y, Ohkubo K, Mohri T, Suzuki T. Thermal conductivity of Ni_3X and Pt_3X in ordered and disordered states. Mater Sci Eng A 1997;239–240:907–14.

[20] Terada Y, Ohkubo K, Mohri T, Suzuki T. Thermal conductivity of Ni_3Al with ternary additions. Mater Sci Eng A 2001;311:232–5.

[21] Shirai Y, Masaki K, Inoue T, Nishitani SR, Yamaguchi M. Electrical resistivity of Ll_2 trialuminides containing 3*d* transition element. Intermetallics 1995;3: 381–8.

[22] Mooij JH. Electrical conduction in concentrated disordered transition metal alloys. Phys Status Solidi A 1973;17:521–30.

[23] Miyake J, Fine ME. Electrical conductivity versus strength in a precipitation hardened alloy. Acta Metall 1992;40:733–41.

[24] Hitchcock AH. The Hall coefficient and deviations from Nordheim's rule in a-phase copper alloys. Phys Let 1971;35A:80–1.

[25] Landauer R. The electrical resistance of binary metallic mixtures. J Appl Phys 1952;23:779–84.

[26] Zheng X, Cahill DG, Krasnochtchekov P, Averback RS, Zhao JC. High-throughput thermal conductivity measurements of nickel solid solutions and the applicability of the Wiedemann–Franz law. Acta Mater 2007;55: 5177–85.